# Establishment of a National Primary Standard for Air Speed up to 90 m/s at NMIJ

**A. Iwai[1], T. Funaki[1], N. Kurihara[1] and Y. Terao[1]**

*[1]National Metrology Institute of Japan (NMIJ),*
*National Institute of Advanced Industrial Science and Technology (AIST),*
*1-1-1 Umezono, Tsukuba, Ibaraki 305-8563, Japan*
*E-mail (corresponding author): a.iwai@aist.go.jp*

**Abstract**

NMIJ has established a high air speed standard facility and has been providing a calibration service since April 2015. The facility has an air speed range of 40 to 90 m/s with a relative expanded uncertainty ($k$ = 2) of 0.63%. The purpose of this primary standard is mainly to contribute to the improvement of meteorological observation and research. The reference air speed is derived from the national primary gas flowrate standard of Japan. The contraction nozzle for conversion from flowrate to air speed is installed at the test line of the closed loop gas flowrate calibration facility. The standard air speed at the nozzle exit is obtained by comparing the integral value of the air speed profile and the standard gas flowrate. The total pressure tube used as a transfer standard is then calibrated against the standard air speed at the nozzle exit. Using this total pressure tube, the Eiffel-type wind tunnel, which is a working standard for the daily calibration service, is calibrated. The present paper describes the calibration system, the traceability chain, and the uncertainty analysis of the new air speed standard.

## 1. Introduction

Air speed is important as a quantitative index used for the assessment of building wind-resistance, indoor thermal environments, and the aerodynamic characteristics of high-speed vehicles. In order to investigate the emission volume of greenhouse gases, improvement of the air speed measurement method for chimneystack flow and exhaust air duct flow is necessary. Moreover, there is also interest in risk assessment of wind disasters due to typhoons and gusts. Because of the characteristics of the climate of Japan, such applications require testing at air speeds of up to 90 m/s. NMIJ had the wide range of the air speed standard, that was limited range up to 40 m/s[1][2][3][4].

In above reason, NMIJ began to develop an air speed standard facility for air speeds exceeding 40 m/s. Generally, a laser Doppler velocimeter (LDV) is used as the air speed standard measurement device. However, because of the instability of the scattering particle density and the LDV signal in the high air speed range [5], the reference air speed is derived from the national primary gas flowrate standard of Japan. The standard procedure involves air speed measurement at the center of the jet and comparison of the standard volume flowrate, and the integral value of the air speed profile.

## 2. Facility

The high air speed standard facility consists of a closed-loop flowmeter calibration facility [6] and a high air speed calibration wind tunnel. The former is the primary standard of gas flowrate, and the latter is a working standard for the daily calibration service. Figures 1(a) and 1(b) show schematic diagrams of the closed-loop flowmeter calibration facility and the flowrate-to-air-speed conversion device. Figure 2 shows a schematic diagram of the high air speed calibration wind tunnel.

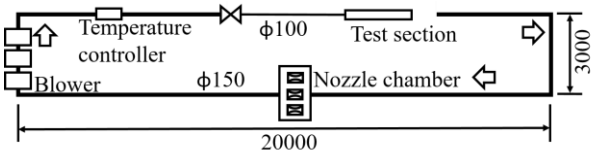


**Figure 1(a):** Closed-loop flowmeter calibration facility.

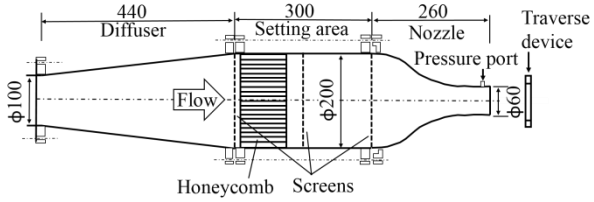


**Figure 1(b):** Flowrate-to-air-speed conversion device positioned at the test section.

The closed-loop flowmeter calibration facility includes a nozzle chamber, a blower, a temperature controller, and flowmeter test lines and provides a volume flowrate of up to 1,000 $m^3$/h with a relative expanded uncertainty ($k$ = 2) of 0.28 % in the test line. The test section is

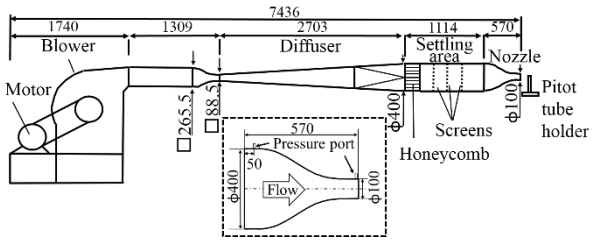


**Figure 2:** Schematic diagram of the high air speed calibration wind tunnel. The inset (dashed rectangle) shows a detailed diagram of the nozzle.

located in the 100 mm test line. The area between the nozzle and the downstream test line is open to the test room.

The test section consists of a diffuser, a settling area, a nozzle, and a traverse device. As shown in Figure 1(b), the diffuser expands the test line diameter from 100 mm to 200 mm, and the settling area with a diameter of 200 mm contains three screens and one honeycomb. The outlet diameter of the nozzle is 60 mm, and the nozzle ratio is 1:12.25. The nozzle profile is modeled with a cubic polynomial model [7]. The jet is stable, and the air speed profile at the nozzle center is almost flat. The pressure port is located 20 mm upstream from the nozzle exit, and the pressure at this location is the standard pressure during measurement of the total and static pressures. The traverse device has two degrees of freedom in polar coordinates and holds a hot-wire anemometer, a total pressure tube (TPT) or a static pressure tube (SPT). The test room temperature is maintained at 24.5 °C ± 1 °C by a special air conditioning unit, and the flow temperature is maintained at 24.5 °C ± 0.3 °C by the temperature controller.

The high air speed calibration wind tunnel is an Eiffel-type wind tunnel with a total length of approximately 8.2 m. The wind tunnel consists of a blower, a diffuser, a settling area, and a nozzle. The settling area, which has a diameter of 400 mm, contains three screens and one honeycomb. The outlet diameter of the nozzle is 100 mm, and the nozzle ratio is 1:16. The nozzle length is 570 mm from inlet to outlet. Pressure ports are located at the nozzle inlet and outlet, and the nozzle outlet pressure is the standard pressure during total and static pressure measurements. During air speed measurement, the test room temperature is 18 °C ± 3 °C. For an air speed setting of 90 m/s, the jet flow temperature increases approximately 25 °C because of the blower heat.

## 3. Setup procedure of the standard air speed

### *3.1 Outline of the setup procedure*

The setup procedure consists of three steps, as outlined by the traceability chain in Figure 3.

First, the standard air speed at the nozzle exit was obtained by comparing the integral value of the air speed profile and the standard gas flowrate. The TPT is constructed of stainless steel and has an outer diameter of 3 mm and a tip diameter of 1 mm, was used as a transfer standard and was calibrated against the standard air speed at the nozzle exit. Using the TPT, the pressure difference between the nozzle inlet and outlet at the wind tunnel was calibrated, and the air speed coefficient was obtained. Finally, using the pressure difference and the air speed coefficient, the pressure difference obtained by the Pitot-static tube, as the device under test (DUT), was calibrated and the Pitot coefficient was obtained.

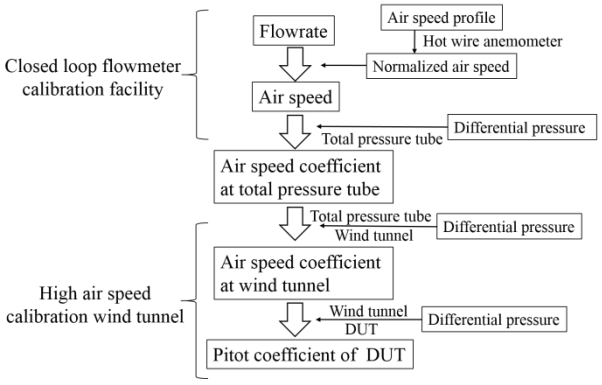


**Figure 3:** Traceability chain of the high air speed standard. The DUT is the Pitot-static tube under calibration.

### *3.2 Determination of reference air speed at the closed-loop flowmeter calibration facility*

This section describes how to determine the reference air speed at the closed-loop flowmeter calibration facility. First, the hot-wire anemometer was positioned parallel to the flow direction at the traverse device, and the standard volume flowrate in the test line was programmed as the setting value. After the hot-wire anemometer output voltage was calibrated using the linearizer, the cross-sectional air speed profile on the plane perpendicular to the flow direction was measured 1 mm downstream from the nozzle exit. The standard air speed was determined such that the air speed at the center of the jet was equivalent to the known standard volume flowrate, and the volume flowrate was determined by integrating the air speed profile.

The volume flowrate in the test line was varied as 400 $m^3/h$, 600 $m^3/h$, 800 $m^3/h$, and 1,000 $m^3/h$, which correspond to air speeds at the center of the jet of approximately 40 m/s, 60 m/s, 80 m/s, and 100 m/s respectively. The hot-wire probe is an I-type 55 P11 (Dantec Dynamics A/S). In order to obtain higher-resolution air speed profiles, the wire was aligned with the tangent direction of the nozzle exit. The output voltage was linearized by a linearizer and was sampled for 1 s at a sampling rate of 1 kHz using DL750 ScopeCorder (Yokogawa Meters & Instruments Corporation). A total of eight cross-sectional air speed profiles were obtained at the center of the jet flow for $\theta$ = 0° to 315° at 45° intervals. Each profile contains approximately 30 measurement points at radial intervals of 5 mm starting from the center of the jet, and at intervals of 0.05 mm around the edge of the jet, where

the air speed gradient is high. Figure 4 shows a diagram of the air speed profile measurement method, and Figure 5 shows an example of an obtained profile.

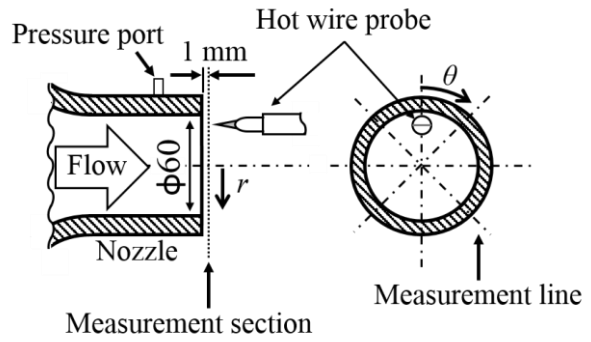


**Figure 4:** Air speed profile measurement method.

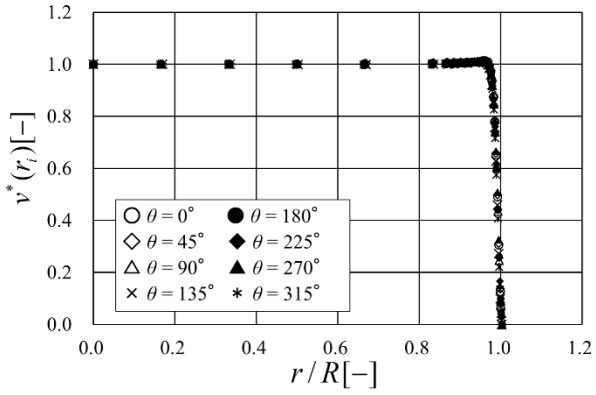


**Figure 5:** Air speed profiles at 400 m³/h.

The local air speed ratio, $v^*(r_i)$, normalized by the air speed at the center of the jet, $v_c$ [m/s], was obtained as follows:

$$v^*(r_i) = \frac{v(r_i)}{v_c} = \frac{E(r_i)}{E_c} \quad . \tag{1}$$

Using $v^*(r_i)$, $v_c$ [m/s] was obtained as follows:

$$v_c = \frac{Q_V}{\pi\left[v^*(r_0)\left(\frac{r_1}{2}\right)^2 + \sum_{i=1}^{e-1} v^*(r_i)\left\{\left(\frac{r_{i+1}+r_i}{2}\right)^2 - \left(\frac{r_i+r_{i-1}}{2}\right)^2\right\}\right]} \quad . \tag{2}$$

Here, $Q_v$ [m³/s] is the standard volume flowrate, $r_i$ is the i-th measurement location point from the center of the jet, the air speed is integrated from $v(r_0)$ to $v(r_{e-1})$, $r_0$ [m] is the center of the jet, and $r_e$ [m] is the end of the jet, so $v(r_e) = 0$. Figure 6 shows the ratio of $v_c$ [m/s] to the bulk velocity $v_{bulk}$, which is the average cross-sectional velocity at the nozzle exit. The error bars in Figure 6 indicate the standard uncertainty obtained from the uncertainty analysis to be described later. Figure 7 shows the air speed profile averaged over the same radial points at each standard volume flowrate setting. As shown in Figure 7, the shear layer becomes thinner at higher air speeds, and $v_c$ approaches $v_{bulk}$, as indicated in Figure 6.

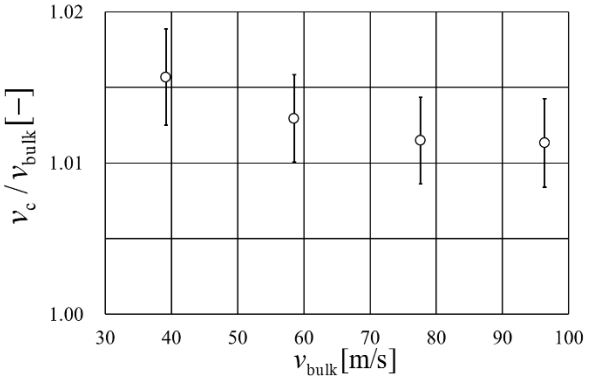


**Figure 6:** Ratio of air speed at the center of the jet to the bulk air speed at the nozzle exit. The error bars indicate standard uncertainty.

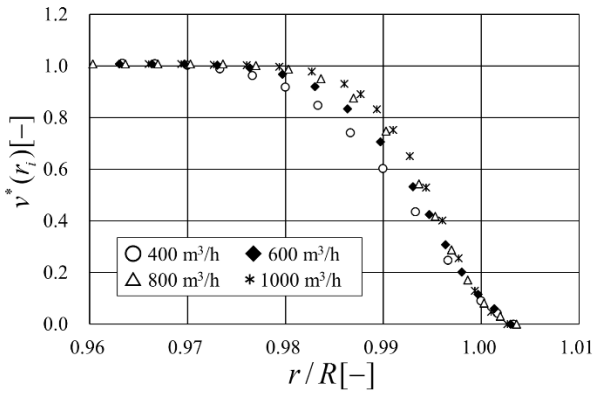


**Figure 7:** Average air speed profile at each volume flowrate.

### *3.3 TPT calibration at the closed-loop flowmeter calibration facility*

This section describes the TPT calibration procedure at the closed-loop flowmeter calibration facility. First, the TPT was aligned with the flow direction on the traverse device so that the front-end is located 1 mm downstream from nozzle exit and at the center of the jet, and the standard volume flowrate in the test line was controlled to the setting value. Next, the pressure difference between the total pressure and the standard pressure from the pressure port at the nozzle exit was measured. The static pressure of the SPT was measured using the same method. Based on the pressure difference and air density at the test section, the air speed value $v_p$ [m/s] of the TPT was calculated using Bernoulli's theorem, as follows:

$$v_{\mathrm{p}} = \sqrt{\frac{2\left(\Delta P_{\mathrm{Ct}} - \Delta P_{\mathrm{Cs}}\right)}{\rho}} \qquad (3)$$

where $\Delta P_{\mathrm{Ct}}$ is the total pressure [Pa], $\Delta P_{\mathrm{Cs}}$ is the static pressure [Pa], and $\rho$ is the air density during the $\Delta P_{\mathrm{Ct}}$ measurement. Finally, based on the ratio of $v_{\mathrm{c}}$ to $v_{\mathrm{p}}$, the correction coefficient of the TPT $C_{\mathrm{t}}$ [-] was calculated as follows:

$$C_{\mathrm{t}} = \frac{v_{\mathrm{c}}}{v_{\mathrm{p}}}. \qquad (4)$$

*3.4 Calculation of the correction coefficient of the wind tunnel using the TPT*

This section describes the wind tunnel calibration procedure. First, the TPT calibrated as described in Section 3.3 was positioned parallel to the flow direction at the center of the jet, and the output of the blower was controlled to the setting value. Second, the pressure difference between the total pressure and the pressure at the nozzle outlet and that between the pressure at the nozzle inlet and the pressure at the nozzle outlet were measured at the same time. The SPT measurement used in the TPT calibration was conducted in a similar manner. Finally, based on the ratio of the differential pressures between the total and static pressures and between the pressures at the nozzle inlet and outlet, the correction coefficient of the wind tunnel $C_{\mathrm{WT}}$ [-] was calculated, as follows:

$$C_{\mathrm{WT}} = C_{\mathrm{t}} \sqrt{\frac{\Delta P_{\mathrm{Nt}} - \Delta P_{\mathrm{Ns}}}{\Delta P_{\mathrm{tWT}}}} \qquad (5)$$

where $\Delta P_{\mathrm{Nt}}$ is the total pressure [Pa], $\Delta P_{\mathrm{Ns}}$ is the static pressure [Pa], and $\Delta P_{\mathrm{tWT}}$ is the pressure difference between the nozzle inlet and the nozzle exit.

*3.5 Calibration of the Pitot-static tube by the high air speed calibration wind tunnel*

This section describes the daily calibration procedure for a DUT, which is a Pitot-static tube. First, the Pitot-static tube was aligned with the flow direction downstream of the nozzle exit, and the output of the blower was controlled to the setting value. The differential pressures of the Pitot-static tube and the nozzle were then measured simultaneously. Finally, based on the ratio of these differential pressures, the Pitot coefficient $C_{\mathrm{pit}}$ [-] was calculated as follows:

$$C_{\mathrm{pit}} = C_{\mathrm{WT}} \sqrt{\frac{\Delta P_{\mathrm{WTp}}}{\Delta P_{\mathrm{pit}}}} \qquad (6)$$

where $\Delta P_{\mathrm{pit}}$ is the differential pressure of the DUT and $\Delta P_{\mathrm{WTp}}$ is the differential pressure of the nozzle. The calibration results and validity evaluation are described in the following section.

## 4. Uncertainty analysis

*4.1 Model formula of the uncertainty*

The standard uncertainty of the Pitot coefficient for the DUT is given by the following equation based on the propagation formula of the uncertainty [8]:

$$\begin{aligned}
&\left(\frac{u_{\mathrm{c}}\left(C_{\mathrm{pit}}\right)}{C_{\mathrm{pit}}}\right)^2 \\
&= \left(\frac{\partial C_{\mathrm{pit}}}{\partial C_{\mathrm{WT}}}\right)^2 \left(\frac{u\left(C_{\mathrm{WT}}\right)}{C_{\mathrm{pit}}}\right)^2 + \left(\frac{\partial C_{\mathrm{pit}}}{\partial \Delta P_{\mathrm{WTp}}}\right)^2 \left(\frac{u\left(\Delta P_{\mathrm{WTp}}\right)}{C_{\mathrm{pit}}}\right)^2 + \left(\frac{\partial C_{\mathrm{pit}}}{\partial \Delta P_{\mathrm{pit}}}\right)^2 \left(\frac{u\left(\Delta P_{\mathrm{pit}}\right)}{C_{\mathrm{pit}}}\right)^2 \\
&= \left(\frac{u\left(C_{\mathrm{WT}}\right)}{C_{\mathrm{WT}}}\right)^2 + \left(\frac{1}{2}\right)^2 \times \left(\frac{u\left(\Delta P_{\mathrm{WTp}}\right)}{\Delta P_{\mathrm{WTp}}}\right)^2 + \left(\frac{1}{2}\right)^2 \times \left(\frac{u\left(\Delta P_{\mathrm{pit}}\right)}{\Delta P_{\mathrm{pit}}}\right)^2 \\
&= \underbrace{\left(\frac{u\left(v_{\mathrm{c}}\right)}{v_{\mathrm{c}}}\right)^2}_{(a_0)} + \underbrace{\left(\frac{u\left(v_{\mathrm{p}}\right)}{v_{\mathrm{p}}}\right)^2}_{(b_0)} + \underbrace{\left(\frac{1}{2}\right)^2 \times \left(\frac{u\left(\Delta P_{\mathrm{tWT}}\right)}{\Delta P_{\mathrm{tWT}}}\right)^2}_{(c)} + \underbrace{\left(\frac{1}{2}\right)^2 \times \left(\frac{u\left(\Delta P_{\mathrm{Nt}} - \Delta P_{\mathrm{Ns}}\right)}{\Delta P_{\mathrm{Nt}} - \Delta P_{\mathrm{Ns}}}\right)^2}_{(d)} \\
&+ \underbrace{\left(\frac{1}{2}\right)^2 \times \left(\frac{u\left(\Delta P_{\mathrm{WTp}}\right)}{\Delta P_{\mathrm{WTp}}}\right)^2}_{(e)} + \underbrace{\left(\frac{1}{2}\right)^2 \times \left(\frac{u\left(\Delta P_{\mathrm{pit}}\right)}{\Delta P_{\mathrm{pit}}}\right)^2}_{(f)}
\end{aligned} \qquad (7)$$

where $u\left(X\right)$ is the standard uncertainty of the measured $X$, and $u_{\mathrm{c}}\left(C_{\mathrm{pit}}\right)$ is the combined standard uncertainty of the Pitot coefficient of a DUT.

The first and second terms of Equation (7) are estimated as follows:

$$\left(\frac{u\left(v_{\mathrm{c}}\right)}{v_{\mathrm{c}}}\right)^2 = \underbrace{\left(\frac{u\left(Q_{\mathrm{V}}\right)}{Q_{\mathrm{V}}}\right)^2}_{(a_1)} + \underbrace{\left(\frac{u\left(\pi\left[v^*(r_0)\left(\frac{r_1}{2}\right)^2 + \sum_{i=1}^{e-1} v^*(r_i)\left\{\left(\frac{r_{i+1}+r_i}{2}\right)^2 - \left(\frac{r_i+r_{i-1}}{2}\right)^2\right\}\right]\right)}{\pi\left[v^*(r_0)\left(\frac{r_1}{2}\right)^2 + \sum_{i=1}^{e-1} v^*(r_i)\left\{\left(\frac{r_{i+1}+r_i}{2}\right)^2 - \left(\frac{r_i+r_{i-1}}{2}\right)^2\right\}\right]}\right)^2}_{(a_2)} \qquad (8)$$

$$\left(\frac{u\left(v_{\mathrm{p}}\right)}{v_{\mathrm{p}}}\right)^2 = \underbrace{\left(\frac{1}{2}\right)^2 \times \left(\frac{u\left(\Delta P_{\mathrm{Ct}} - \Delta P_{\mathrm{Cs}}\right)}{\Delta P_{\mathrm{Ct}} - \Delta P_{\mathrm{Cs}}}\right)^2}_{(b_1)} + \underbrace{\left(-\frac{1}{2}\right)^2 \times \left(\frac{u\left(\rho\right)}{\rho}\right)^2}_{(b_2)} \qquad (9)$$

*4.2 Calculation of the relative expanded uncertainty*

The combined standard uncertainty of the Pitot coefficient was obtained as follows:

$$\frac{u_c(C_{pit})}{C_{pit}} = 0.316\times10^{-2}. \quad (10)$$

When the coverage factor is 2, the relative standard uncertainty is obtained as follows:

$$\frac{U(C_{pit})}{C_{pit}} = k\frac{u_c(C_{pit})}{C_{pit}} = 2\times0.316\times10^{-2} \fallingdotseq 0.63\times10^{-2}. \quad (11)$$

The uncertainty sources and uncertainties are listed in Table 1. The largest uncertainty factor is the standard volume flowrate. In order to improve the total accuracy, increased flowrate by entrainment of the air surrounding the jet have to be evaluated more precisely. The second largest uncertainty factor is the air speed profile measurement. In order to address this problem, the increase of the number of the repeated measurement and the high precision of the calibration coefficient by the air speed of the hot-wire anemometer should investigate.

**Table 1:** Uncertainty sources and standard uncertainties.

| Uncertainty sources | | Standard uncertainty | Sensitivity coefficient |
|---|---|---|---|
| Standard volume flow rate | | 0.223 % | 1 |
| Velocity distribution | | 0.218 % | 1 |
| Velocity by the total pressure tube | | 0.032 % | 1 |
| Differential pressure by the total pressure tube | | 0.050 % | 0.5 |
| Differential pressure by the nozzle | | 0.037 % | -0.5 |
| At calibration | Differential pressure by the nozzle | 0.036 % | 0.5 |
| | Differential pressure by DUT | 0.039 % | -0.5 |
| | | | |
| Combined standard uncertainty | | 0.316 % | |
| Expanded uncertainty ($k$ = 2) | | 0.63 % | |

*4.3 Validation*

The calibration results based on the procedure described above were validated experimentally. The JIS type Pitot static tube was used as a transfer standard and was calibrated both at the present high air speed calibration wind tunnel and at the medium air speed calibration wind tunnel at 40 m/s. The medium air speed calibration wind tunnel has been used for calibration service for almost 20 years and its relative expand uncertainty ($k$ = 2) is 0.35 %. The validity of the medium air speed standard was confirmed through intercomparison with NMIs around the world[9][10].

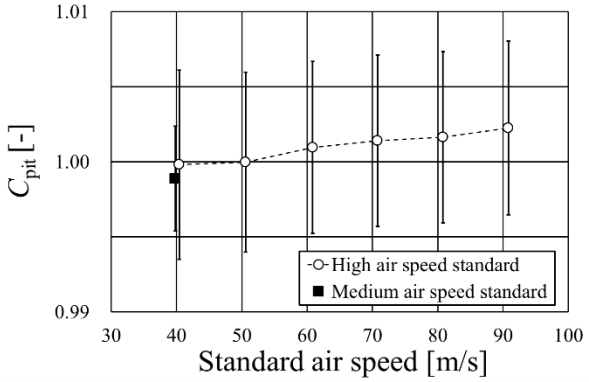


**Figure 8:** High air speed standard and medium air speed standard at 40 m/s. The error bars indicate the relative expanded uncertainty ($k$ = 2).

The calibration results for the DUT are shown in Figure 8. As shown in this figure, the Pitot coefficient is approximately 1 and increases slightly with the increasing air speed. Moreover, the difference between the Pitot coefficients for the medium and high air speed standards at 40 m/s is very small compared to the relative expanded uncertainty. Thus, the validity of the high air speed standard was confirmed.

## 5. Conclusion

NMIJ has established a new primary standard of high air speed, for which the air speed ranges from 40 m/s up to 90 m/s with a relative expanded uncertainty ($k$ = 2) of 0.63%. Based on in-house comparisons with the medium air speed standard, the validity of the high air speed standard was confirmed. The major sources of uncertainty for the standard are the standard volume flowrate and the air speed profile measured by the hot-wire anemometer. The improvement of these error factors is a subject for further investigation.

## References


[1] Terao, Y. and Takamoto, M., "Low Velocity Standard for Air Flow Using a Towing Carriage", *Transaction of the Society of Instrument and Control Engineers*, **Vol.**26, No.1, pp. 1-8, 1990. (in Japanese)

[2] Terao, Y., Takamoto, M., and Mattingly, G. E., "Preliminary Intercomparison of Anemometer Calibration Systems at Very Low Speeds between the National Standard Laboratories in Japan and the USA", *JSME International Journal Series B*, **Vol**. 40, No.3, pp. 509-515, 1997.

[3] Terao,Y., "Study on Measurement Standard of Very Low Air Speed", *Bulletin of NRLM*, **Vol**.47, Supplement No. 196, pp.217-256, 1998. (in Japanese)

[4] Kurihara, N., Terao, Y., Nakao, S., and Takamoto, M., "An Uncertainty of Laser Doppler Velocimeter Calibration for Air Speed Standard", *Transactions of the Japan Society of Mechanical Engineers, Series B*, **Vol**.71, No.708, pp. 2100-2107, 2005. (in Japanese)

[5] Japan Society of Mechanical Engineers, *JSME Data Book: Flow Measurements* (Tokyo, JSME), pp. 142-145, 1985. (in Japanese)

[6] Ishibashi, M. and Morioka, T., "The renewed airflow standard system in Japan for 5-1000 $m^3/h$", *Flow Measurement and Instrumentation*, **Vol**.17, Issue 3, pp.153-161, 2006.

[7] Rouse, H. and Hassan, M. M.: "Cavitation-Free Inlets and Contractions", *Mechanical. Engineering.*, **Vol**. 71, pp. 213-216, 1949.

[8] ISO Guide 98-3: *Guide to the Expression of Uncertainty in Measurement*, 2008.

[9] Terao et al., "Final report on the CIPM air speed key comparison (CCM.FF-K3)", *Metrologia*, **Vol**. 44, Technical Supplement 07009, 2007.

[10] Terao et al., "Final report on the APMP air speed key comparison (APMP.M.FF-K3), *Metrologia*, **Vol**. 47, Technical Supplement 07012, 2010.